Infrared spectroscopy of endohedral HD and D_2 in C_[60]

Ge, Min; Nagel, U.; Huevonen, D.; Room, T.; Mamone, S.; Levitt, M. H.; Carravetta, M.; ... Komatsu, K.; Lei, Xuegong; Turro, N. J.

Infrared spectroscopy of endohedral HD and D2 in C60

Min Ge, U. Nagel, D. Hüvonen, T. Rõõm, S. Mamone et al.

Citation: J. Chem. Phys. **135**, 114511 (2011); doi: 10.1063/1.3637948
View online: http://dx.doi.org/10.1063/1.3637948
View Table of Contents: http://jcp.aip.org/resource/1/JCPSA6/v135/i11
Published by the American Institute of Physics.

THE JOURNAL OF CHEMICAL PHYSICS **135**, 114511 (2011)

Infrared spectroscopy of endohedral HD and D_2 in C_{60}

Min Ge, U. Nagel,[1] D. Hüvonen,[1] T. Rõõm,[1,a)] S. Mamone,[2] M. H. Levitt,[2] M. Carravetta,[2] Y. Murata,[3] K. Komatsu,[3] Xuegong Lei,[4] and N. J. Turro[4]
[1]*National Institute of Chemical Physics and Biophysics, Akadeemia tee 23, 12618 Tallinn, Estonia*
[2]*School of Chemistry, Southampton University, Southampton SO17 1BJ, United Kingdom*
[3]*Institute for Chemical Research, Kyoto University, Kyoto 611-0011, Japan*
[4]*Department of Chemistry, Columbia University, New York, New York 10027, USA*

(Received 1 July 2011; accepted 22 August 2011; published online 20 September 2011)

We report on the dynamics of two hydrogen isotopomers, D_2 and HD, trapped in the molecular cages of a fullerene C_{60} molecule. We measured the infrared spectra and analyzed them using a spherical potential for a vibrating rotor. The potential, vibration-rotation Hamiltonian, and dipole moment parameters are compared with previously studied $H_2@C_{60}$ parameters [M. Ge, U. Nagel, D. Hüvonen, T. Rõõm, S. Mamone, M. H. Levitt, M. Carravetta, Y. Murata, K. Komatsu, J. Y.-C. Chen, and N. J. Turro, J. Chem. Phys. **134**, 054507 (2011)]. The isotropic part of the potential is similar for all three isotopomers. In $HD@C_{60}$, we observe mixing of the rotational states and an interference effect of the dipole moment terms due to the displacement of the HD rotation center from the fullerene cage center. © *2011 American Institute of Physics*. [doi:10.1063/1.3637948]

I. INTRODUCTION

Trapping of the hydrogen molecule inside the C_{60} molecular cage by means of chemical methods has created a system where the simplest and the lightest molecule is enclosed in the cavity of a molecule with the highest symmetry.[1,2] The simplicity makes this supra-molecular complex ideal for the studies of non-covalent bondings between H_2 and carbon nano-surfaces, the knowledge needed for the design of carbon-based hydrogen storage materials. $H_2@C_{60}$ is simple from the theoretical point of view – the high symmetry of C_{60} brings it to the level of a quantum mechanics textbook example of a vibrating rotor trapped in a spherical potential well.[3] From the experimental point of view all the trapping sites are equal and there is only one H_2 per trapping site. This minimizes the inhomogeneous line broadening effects and H_2–H_2 interactions. Indeed, the infrared (IR) absorption lines are well separated and show splittings due to translation-rotation coupling,[4] consistent with theoretical predictions.[5–7] The rotational quantum number J is still a good quantum number for H_2 despite the translation-rotation coupling.[7,8] The potential parameters of $H_2@C_{60}$ have been determined in both ground and excited vibrational states from the detailed temperature dependence study of IR spectra[9] and in the ground state by inelastic neutron scattering (INS) spectroscopy.[10] The introduction of a three site Lennard-Jones potential in the pairwise additive five-dimensional potential energy surface has improved greatly the accuracy of quantum calculations of the coupled translation and rotation eigenstates of H_2.[11] In general, it has been established that H_2 inside the C_{60} cage is an unhindered vibrating rotor performing coupled translations and rotations in a nearly spherical potential.[12]

The substitution of deuterium for H changes the energy levels of the encapsulated molecule drastically. In $D_2@C_{60}$, the distances between the energy levels in the vibrational, rotational, and translational manifolds are reduced because of the heavier mass of D. Quantum statistics plays an important role in the dihydrogen wavefunction symmetry.[13] The nucleus of D is a boson (nuclear spin $I = 1$) as opposed to H, where it is a fermion, $I = 1/2$. Thus the rotational states with an even quantum number J have D_2 in the state where the total nuclear spin of D_2 is either zero or two. This is called *ortho*-D_2, while *para*-D_2 has the total nuclear spin one and odd J values. The *ortho-para* ratio at room temperature is 2 : 1 for D_2. As in the case of H_2, the conversion between *ortho* and *para* species is very slow. This means that at liquid helium temperature (4.2 K) we have only two times more J even (*ortho*) than J odd (*para*) D_2 although the $J = 0$ state lies $E/k_B = 84$ K below the $J = 1$ state. This is in sharp contrast with H_2 where the J even (*para*) species are outnumbered by the J odd (*ortho*-H_2) species by three times. Even though the hydrogen molecule is protected by C_{60} the *ortho-para* conversion rate can be enhanced using a spin catalyst.[14] The converted $H_2@C_{60}$ sample, *para*-enriched at 77 K with molecular oxygen as a spin catalyst,[15] was used to identify *para* and *ortho* absorption lines in the infrared spectra.[9]

The energy levels of heteronuclear $HD@C_{60}$ are compressed compared to $H_2@C_{60}$ as well. However, an additional effect appears, the breaking of two symmetries. First, the inversion symmetry of the diatomic molecule is lost. The consequence is that the center of mass is shifted away from the geometric center and a dipole moment is allowed for rotational transitions, $\Delta J = \pm 1$. Second, there are no *ortho* and *para* species since the nuclei of the HD molecule are not identical particles. The consequence is that thermal relaxation between even and odd J levels is fast. All the rotational and translational levels of $HD@C_{60}$ are in thermal equilibrium and at liquid helium temperature only one state with $J = N = 0$, is populated. N is the translational quantum number of the spherical oscillator.[3]

a)Electronic mail: toomas.room@kbfi.ee.

The dynamics of endohedral D_2 and HD has been studied theoretically[8] and of HD experimentally.[10] Three transitions, $N = 0 \rightarrow 1$, $J = 0 \rightarrow 1$, and $J = 1 \rightarrow 2$, were detected by INS spectroscopy.[10] An interesting finding is that the energies of two rotary transitions do not scale according to the energies of a free rotor. This was predicted by Olthof *et al.* in the theoretical study of CO@C_{60}.[16] Simultaneous rotations of CO and its position vector **R** give rise to a rotational structure similar to that of free CO, but the effective rotational constants differ considerably. As theory predicts, the different J and N states are strongly mixed because of the translation-rotation coupling between the heteronuclear rotor and the inner walls of C_{60} making J not a good quantum number as it is for a homonuclear diatomic in C_{60}.[8,16]

This paper is a continuation of our IR studies of H_2@C_{60}.[9] We present and analyze the IR spectra of D_2@C_{60} and HD@C_{60} and compare the potential, vibrating rotor and dipole moment parameters of the three isotopomers.

II. THEORY

The model Hamiltonian of the vibrating rotor in the spherical potential, the dipole moment expansion, the calculation of IR absorption line intensities, and the fitting of IR spectra were described in Ref. 9. Here, we outline the consequences of the reduced symmetry of heteronuclear HD as compared to homonuclear H_2 and D_2. The coordinate $\mathbf{R} = \{R, \Omega\}$ refers to the center of mass displacement of the dihydrogen from the geometric center of C_{60} and the rotational eigenstates $|JM_J\rangle$ are in the coordinate frame $\mathbf{s} = \{s, \Omega_s\}$, where the diatomic rotates about its center of mass and **s** connects the two nuclei of the hydrogen molecule.

The potential transforms according to the A_{1g} irreducible representation of the symmetry group I_h. The bipolar spherical harmonics $F^{lj}_{\lambda m_\lambda}(\Omega, \Omega_s)$ (Eq. (2) in Ref. 9) of the order $\lambda = 0, 6, 10, \ldots$ transform according to the irreducible representation A_{1g} of the symmetry group I_h.[17] We consider the case of full spherical symmetry, $\lambda = 0$. If $\lambda = 0$, then from the triangle rule $\lambda = |l - j|, |l - j| + 1, \ldots, l + j$ it follows that $j = l$.

We write the potential energy for a diatomic molecule as ${}^{v}V = {}^{v}V^0 + {}^{v}V'$, where the isotropic harmonic term is given by ${}^{v}V^0 = {}^{v}V^{002}_{00} R^2 F^{00}_{00}$.[9] We expand the perturbation part of the potential ${}^{v}V'$ in spherical harmonics $F^{lj}_{\lambda m_\lambda}$ and in power series of R,

$$\begin{aligned} {}^{v}V' = {} & {}^{v}V^{004}_{00} R^4 F^{00}_{00} \\ & + \left({}^{v}V^{111}_{00} R + {}^{v}V^{113}_{00} R^3\right) F^{11}_{00} \\ & + \left({}^{v}V^{222}_{00} R^2 + {}^{v}V^{224}_{00} R^4\right) F^{22}_{00}. \end{aligned} \quad (1)$$

The powers n of the displacement of the center of mass R are determined by l: n has the same parity as l and $n \geq l$. Here, ${}^{v}V^{ljn}_{\lambda m_\lambda}$ are the expansion coefficients and we limit our expansion to $j_{\max} = 2$ and $n_{\max} = 4$. ${}^{v}V^{004}_{00}$ is the anharmonic correction to the isotropic coupling, ${}^{v}V^{002}_{00}$. ${}^{v}V^{224}_{00}$ is the anharmonic correction to the anisotropic (translation-rotation) coupling ${}^{v}V^{222}_{00}$. In the HD@C_{60} potential, we have additional anisotropic coupling terms ${}^{v}V^{111}_{00}$ and ${}^{v}V^{113}_{00}$, that are absent in the H_2@C_{60} and D_2@C_{60} perturbation potential, Eq. (7) in Ref. 9.

We express the induced part of the dipole moment as an interaction between H_2 and C_{60} instead of summation over 60 pairwise induced dipole moments between H_2 and carbon atom as was done in Ref. 9. We write the expansion of the dipole moment from the vibrational state v to v' in bipolar spherical harmonics and in power series of R as

$$d_{v'v}(\mathbf{R}, \Omega_s) = \frac{4\pi}{\sqrt{3}} \sum_{l,j,n} {}^{v'v}A^{ljn}_{\lambda m_\lambda} R^n F^{lj}_{\lambda m_\lambda}(\Omega, \Omega_s). \quad (2)$$

The dipole moment transforms according to the irreducible representation T_{1u} of the symmetry group I_h. The spherical harmonics of the order $\lambda = 1, 5, 7, \ldots$ transform according to T_{1u} of the symmetry group I_h.[17] We use $\lambda = 1$ and are interested in $v = 0 \rightarrow 1$ transitions. In spherical symmetry it is sufficient to calculate one component of the dipole moment vector (Eq. (17) in Ref. 9), $m_\lambda = 0$, and if we drop the explicit dependence of $d_{v'v}$ on v, v' and of ${}^{v'v}A^{ljn}_{\lambda m_\lambda}$ on v, v', λ, m_λ, the $m_\lambda = 0$ component of the dipole moment reads

$$d_0(\mathbf{R}, \Omega_s) = \frac{4\pi}{\sqrt{3}} \sum_{l,j,n} A^{ljn} R^n F^{lj}_{10}(\Omega, \Omega_s). \quad (3)$$

As $\lambda = |l - j|, |l - j| + 1, \ldots, l + j$ and $\lambda = 1$ it must be that $l = |j \pm 1|$. The possible combinations are $(lj) \in \{(01), (10), (12), (21), (23), \ldots\}$. If we restrict the expansion up to $n_{\max} = l_{\max} = 1$, we get

$$\begin{aligned} d_0(\mathbf{R}, \Omega_s) = {} & \frac{4\pi}{\sqrt{3}} A^{010} F^{01}_{10} \\ & + \frac{4\pi}{\sqrt{3}} \left(A^{101} F^{10}_{10} + A^{121} F^{12}_{10}\right) R. \end{aligned} \quad (4)$$

Here, A^{010} is zero for homonuclear diatomic molecules. It describes the sum of permanent and induced rotational dipole moments, selection rule $\Delta N = 0, \Delta J = 0, \pm 1$, but $J = 0 \rightarrow 0$ is forbidden. The expansion coefficient A^{101} describes the induced dipole moment that is independent of the orientation of the diatomic molecular axis **s**, selection rule $\Delta N = 0, \pm 1, \Delta J = 0$, but $N = 0 \rightarrow 0$ is forbidden. A^{121} describes the induced dipole moment that depends on the orientation of **s**, $\Delta N = 0, \pm 1$, $\Delta J = 0, \pm 2$, but $N = 0 \rightarrow 0$ and $J = 0 \rightarrow 0$ are both forbidden. All terms in Eq. (4) satisfy the selection rule $\Delta\Lambda = 0, \pm 1$, but $\Lambda = 0 \rightarrow 0$ is forbidden. Λ is the total angular momentum ($\mathbf{\Lambda} = \mathbf{L} + \mathbf{J}$) quantum number and L is the orbital angular momentum quantum number of the spherical oscillator.[3]

The procedure of fitting IR spectra was described in detail in Ref. 9. The values of quantum numbers we used to define the eigenstates $|vJNL\Lambda\rangle$ were $v = 0$ and 1, $J \leq 4$, and $N \leq 7$ for D_2@C_{60}, $J \leq 4$, and $N \leq 6$ for HD@C_{60}. There are 292 *para*-D_2, 404 *ortho*-D_2, and 524 HD states in the selected bases. Energy levels and observed transitions are sketched in Figs. 1 and 2.

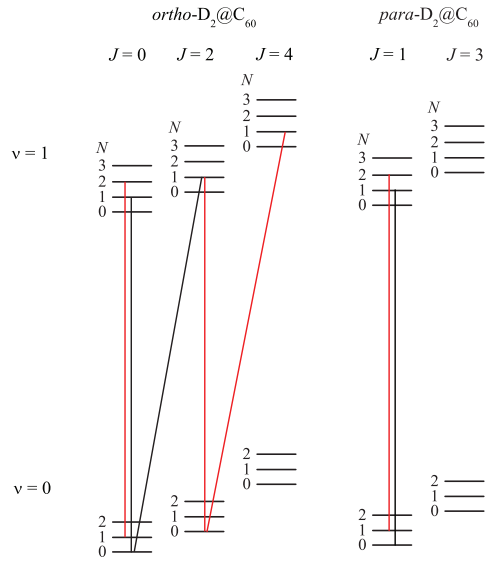

FIG. 1. Diagram of the observed IR transitions of D_2@C_{60}. The rotational quantum number J is even for *ortho*-D_2 states and odd for *para*-D_2 states. Vibrational quantum number is v and translational quantum number is N. The additional structure of energy levels $E^v_{JNL\Lambda}$ due to orbital angular momentum quantum number L and total angular momentum quantum number Λ is not shown and only few lowest values of v, J, and N are represented. Black lines are the transitions that start from the ground state, red lines are the transitions that start from the thermally excited states.

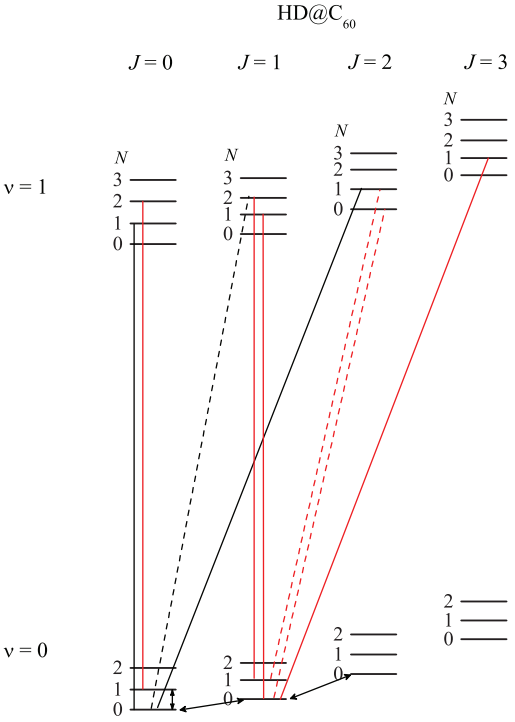

FIG. 2. Diagram of the observed IR transitions of HD@C_{60}. The quantum numbers and the structure of energy levels are same as in Fig. 1. Black lines are the transitions that start from the ground state, red lines are the transitions that start from the thermally excited states. Dashed lines are the unique transitions of HD@C_{60} which have selection rules different from the selection rules of D_2@C_{60} and H_2@C_{60}. Arrow lines are the experimentally observed INS transitions Ref. 10.

III. EXPERIMENT

The endohedral complexes were prepared by "molecular surgery" as described in Refs. 1, 2, D_2@C_{60} at Kyoto University and HD@C_{60} at Kyoto University and Columbia University. The filling factor for D_2 is $\rho = 1.0$. The HD@C_{60} sample was a mixture of the hydrogen isotopomers H_2:HD:D_2 with the ratio 1:1:0.2. Since all C_{60} cages are filled, the filling factor for HD is $\rho = 0.45$. Experimental absorption spectra were corrected for the filling factor. The powdered samples were pressed into pellets under vacuum for IR transmission measurements. The diameter of sample pellets was 3 mm and the thickness $d = 0.25$ mm (D_2@C_{60}) or $d = 0.34$ mm (HD@C_{60}). The measurement technique is described in Ref. 9.

IV. RESULTS

A. Temperature dependence of the spectra

The temperature dependence of the IR absorption spectra of HD@C_{60} and D_2@C_{60} are shown in Figs. 3 and 4. Only the spectral lines involving transitions from the ground translational state, $N = 0$, are present at 5 K. As the temperature is increased, additional lines become visible that correspond to the transitions starting from the excited states, see Figs. 1 and 2. Broad lines that are indicated by arrows in Fig. 3(a) are not due to HD because they are present already at 5 K in the spectral region where only a single line is expected according to our model.

The normalized line areas of D_2, Fig. 4(d) and HD, Fig. 5, are compared to the temperature dependencies of the normalized population probabilities of the corresponding initial states. The population probabilities are calculated using the eigen-energies obtained from fitting the 90 K spectra with the model Hamiltonian. We see that within the error bars the temperature dependence of the normalized line areas is described very well for the transitions starting from $J = 0$ states both in D_2@C_{60} and HD@C_{60}. In HD@C_{60}, the areas of lines that start from $J = 1$ state are weaker than the calculated curve above 120 K. In D_2@C_{60} the intensity versus temperature analysis can be reliably done for one line only, the $N = 0 \rightarrow 1$, $J = 0 \rightarrow 2$ transition at about 3224 cm^{-1}. For other transitions in D_2@C_{60} there is an overlap of spectral lines starting from the ground and thermally populated states or an overlap of *para* and *ortho* lines, see Fig. 6.

The Hamiltonian parameters were determined by fitting the 90 K spectra because at lower temperatures the higher energy levels in the $v = 0$ state are insufficiently populated, while no new lines appear at higher temperatures. The changes in line positions are less than the linewidths over the temperature range explored.

B. Fitting the experimental spectra

There are much fewer observable IR absorption lines in the spectra of D_2@C_{60} and HD@C_{60} than in H_2@C_{60} spectra. The missing lines are the fundamental vibrational transition, $\Delta v = 1$, $\Delta N = \Delta J = 0$ and the group of lines, Δv

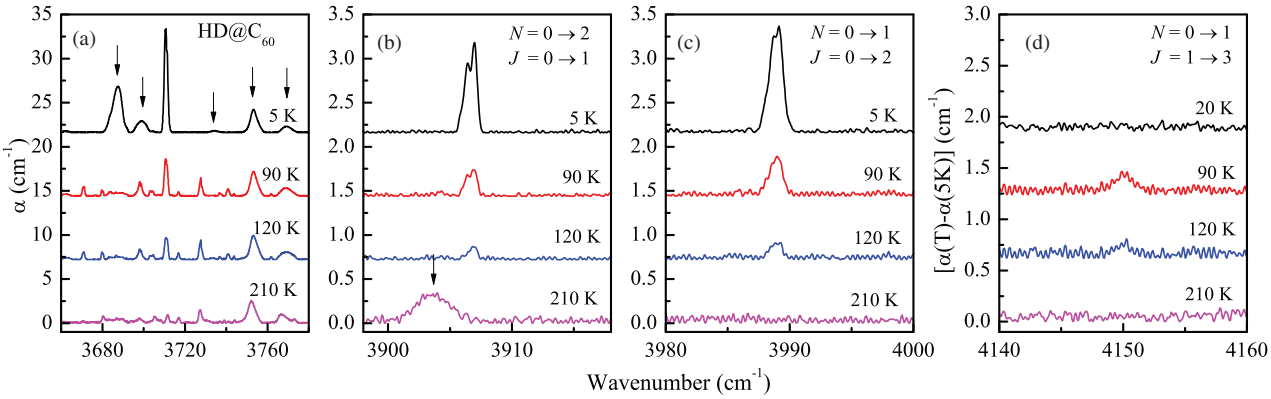

FIG. 3. Temperature dependence of the infrared absorption spectra of HD@C_{60}. In panel (a) the changes of the quantum numbers N and J of the main components of the initial and final states are $\Delta N = 1$, $\Delta J = 0$, or $\Delta N = 0$, $\Delta J = 1$. Panels (b), (c), and (d) show groups of transitions with the same change of the quantum numbers J and N. Spectra are shifted vertically for clarity. The spectra shown in panel (d) are the differential absorption with respect to the 5 K spectrum. The broad lines indicated by arrows are not due to HD.

$= 1$, $\Delta N = -1$, $\Delta J = 0$, placed at lower energies than the fundamental transition. At least some of these lines are needed to determine the vibrational frequency of the diatomic and the difference of the translational potential in the ground ($v = 0$) and excited ($v = 1$) vibrational states.

However, the separation of some energy levels in the ground vibrational state of HD@C_{60} is known from the INS experiment.[10] The numbers we used are $\omega_{N=0\to1} = 154.1\ \text{cm}^{-1}$, $\omega_{J=0\to1} = 80.7\ \text{cm}^{-1}$, and $\omega_{J=1\to2} = 192.0\ \text{cm}^{-1}$. The INS transition frequencies were included in our fitting program.

No additional experimental data beside IR data are available for D_2@C_{60}. Therefore, we estimate the D_2@C_{60} fundamental frequency and set it to a fixed value in our fit of the Hamiltonian parameters. The relative change of the frequency $[\omega_0(\text{gas}) - \omega_0(C_{60})]/\omega_0(\text{gas})$ depends on the cage and is independent of the hydrogen isotopomer.[19] Based on our

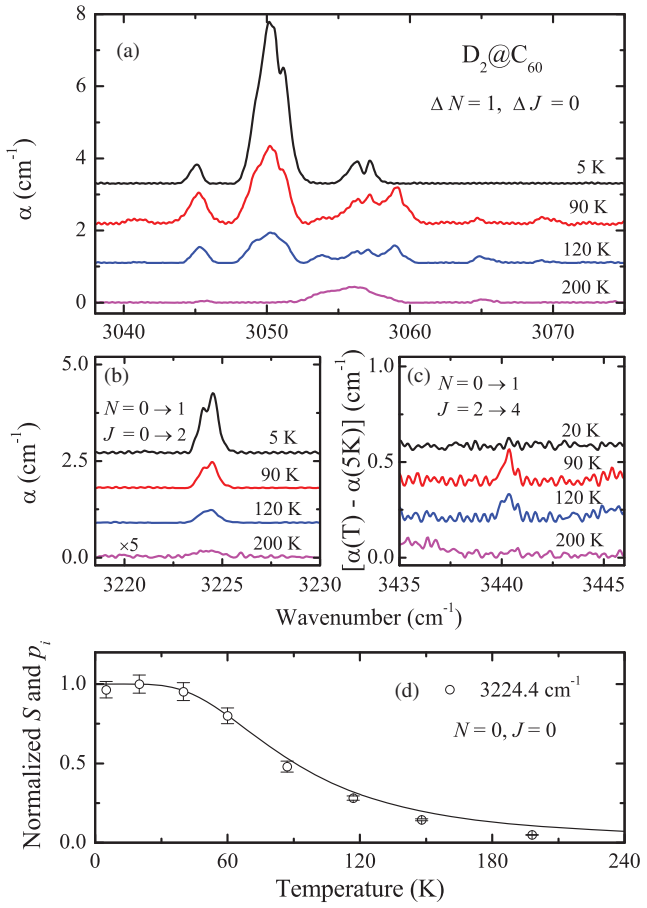

FIG. 4. Temperature dependence of the infrared absorption spectra of D_2@C_{60}. Three panels show groups of transitions with the same change of the quantum numbers J and N. Spectra are shifted vertically for clarity. The 200 K absorption spectra in panel (b) has been multiplied by five. The spectra shown in panel (c) are the differential absorption with respect to the 5 K spectrum. (d) Temperature dependence of the 3224 cm^{-1} IR absorption line normalized area S (circles) and calculated normalized thermal population probability p_i of the initial state $N = J = 0$ (solid line). The error bars of S are from fitting the experimental lines with Gaussians.

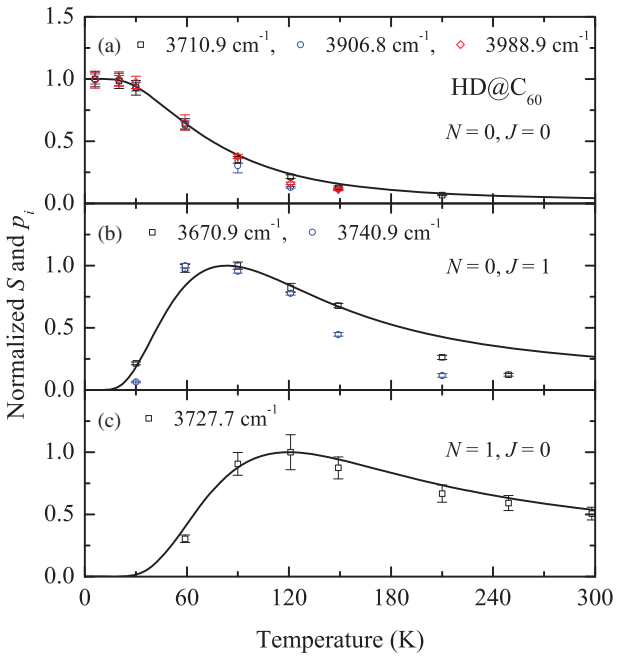

FIG. 5. Temperature dependence of selected IR absorption line areas S of HD@C_{60}. Each panel describes transitions starting from one initial state marked by quantum numbers N and J. Solid lines are calculated thermal population probabilities p_i of the initial states as obtained from the model. S and p_i have been normalized to unity at their maxima. The error bars of S are from fitting the experimental lines with Gaussians.

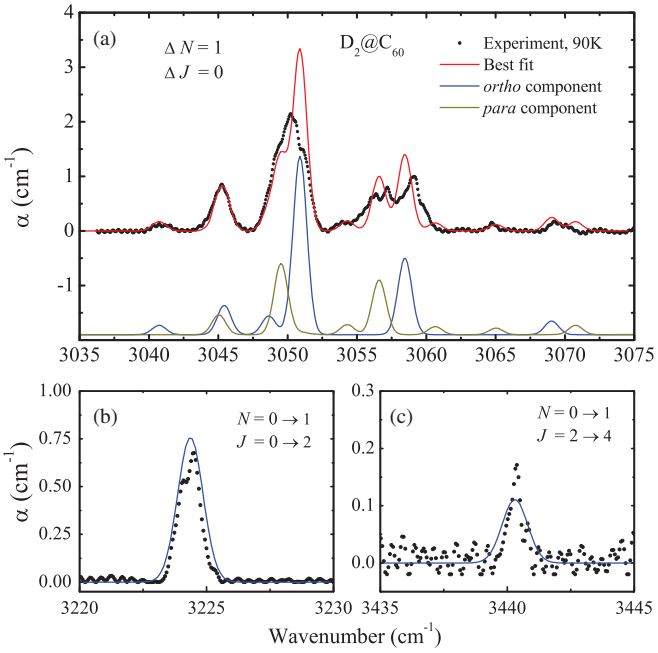

FIG. 6. Experimental absorption spectra of D_2@C_{60} at 90 K (dots) together with the fit result with fixed line width, FWHM = 1 cm^{-1}. The *ortho*-D_2 (blue line) and *para*-D_2 (olive line) components of the fit in panel (a) are shifted down in vertical direction for clarity. The total absorbance α (red line) is the sum of the *ortho*-D_2 and *para*-D_2 spectrum. In panels (b) and (c) the *para* component is not plotted as it does not have any contribution.

fit results, Table VI, we get that for the H_2 $\omega_0(C_{60})/\omega_0(\text{gas}) = 0.9763$ and for the HD $\omega_0(C_{60})/\omega_0(\text{gas}) = 0.9773$. We use the average of these two ratios to calculate the D_2@C_{60} fundamental vibrational frequency, $\omega_0 = 2924$ cm^{-1}.

The line intensities depend on the *ortho-para* ratio, and on the absolute value and relative sign of the dipole moment parameters. We choose $A^{101} > 0$. The line intensities depend on the mixing of pure states by the perturbation part of the potential too. However, the perturbation part can be determined by fitting the IR transition frequencies.

We found that it is not possible to fit independently the two dipole moment parameters and the *ortho-para* ratio in the D_2 sample for the following reasons: first, the number of observed *para* lines is small; second, the strongest low temperature *para* line overlaps with *ortho* line at 3050 cm^{-1}.

The ratio n_o/n_p is close to the high temperature equilibrium value in H_2@C_{60} even at 5 K.[9] Since H_2@C_{60} and D_2@C_{60} were prepared under similar conditions, the *ortho-para* ratio of the D_2 sample in our fitting program was set to the room temperature equilibrium value $n_o/n_p = 2$.

Detailed results of fitting the absorption spectra are shown in Figs. 6 and 7. The experimental and fitted absorption lines are summarized in Tables I and II together with the dominant components of the initial and final eigenstates. Eigenstates are listed in Tables III–V up to the highest states that are involved in the measured infrared transitions of *ortho*-D_2 and HD, and 20 lowest levels of *para*-D_2.

The best fit parameters are listed in Table VI. Because of the limited number of observed lines in the spectra of D_2@C_{60} and HD@C_{60}, we cannot find the anharmonic corrections to the anisotropic confining potential, thus ${}^{v}V_{00}^{224} = 0$. The potential parameters are positive for all three hydrogen isotopomers. The distance between translational levels increases with the quantum number N, if the anharmonic corrections to the isotropic confining potential are greater than zero, ${}^{v}V_{00}^{004} > 0$. In H_2@C_{60} and D_2@C_{60} the sign of ${}^{v}V_{00}^{004}$ also determines the order of L levels for a given N: the lowest energy level has the largest L value. The sign of the translation-rotation coupling ${}^{v}V_{00}^{222}$ determines the order of Λ levels for given J, N, and L, see Table VI. The ordering of L and Λ

TABLE I. Experimental and calculated line positions, ω (cm^{-1}), and absorption line areas, S_ω (cm^{-2}), of IR-active modes at 90 K in D_2@C_{60}. The quantum numbers $JNL\Lambda$ and the relative weights $|\xi^v|^2$ of the main components contributing to the initial and final eigenstates are given. Experimental line positions and areas at 5 K are shown for comparison. The *ortho* and *para* lines at 3050.2 cm^{-1} could not be resolved in the experiment and the total area of the line is listed as experimental S_ω in the corresponding parts of the table.

Experiment, 5 K		Experiment, 90 K		Fitted		Initial state, $v = 0$		Final state, $v = 1$	
ω	S_ω	ω	S_ω	ω	S_ω	$JNL\Lambda$	$\lvert\xi^0\rvert^2$	$JNL\Lambda$	$\lvert\xi^1\rvert^2$
				para lines					
3045.1	0.98	3045.2	1.26	3045.0	0.45	1001	0.99	1111	0.97
3050.2	10.77	3050.2	5.40	3049.5	1.63	1001	0.99	1112	0.96
		3054.0	0.19	3054.3	0.23	1111	0.97	1222	0.93
3056.8	1.55	3056.7	1.81	3056.6	1.26	1001	0.99	1110	0.96
		3060.1	0.11	3060.6	0.19	1111	0.97	1221	0.65
		3064.7	0.11	3065.0	0.15	1110	0.96	1201	0.61
		3069.4	0.21	3070.8	0.21	1112	0.97	1201	0.61
				ortho lines					
		3040.9	0.17	3040.7	0.22	2002	0.99	2112	0.97
		3045.2	1.26	3045.4	0.67	2002	0.99	2113	0.96
				3048.6	0.43	2002	0.99	2111	0.96
3050.2	10.77	3050.2	5.40	3050.9	4.10	0000	0.99	0111	0.96
		3060.1	0.11	3058.5	1.76	0111	0.97	0222	0.93
		3069.4	0.21	3069.0	0.31	0111	0.97	0200	0.88
3224.4	1.66	3224.3	0.86	3224.4	0.95	0000	0.99	2111	0.96
		3440.3	0.09	3440.3	0.14	2002	0.99	4113	0.96

TABLE II. Experimental and calculated line positions, ω (cm^{-1}), and absorption line areas, S_ω (cm^{-2}), of IR-active modes at 90 K in HD@C_{60}. The quantum numbers $JNL\Lambda$ and the relative weights $|\xi^v|^2$ of the main components contributing to the initial and final eigenstates are given. Experimental line positions and areas at 5 K are shown for comparison.

Experiment, 5 K		Experiment, 90 K		Fitted		Initial state, $v=0$		Final state, $v=1$	
ω	S_ω	ω	S_ω	ω	S_ω	$JNL\Lambda$	$\lvert\xi^0\rvert^2$	$JNL\Lambda$	$\lvert\xi^1\rvert^2$
		3670.9	1.67	3670.7	1.57	1001	0.80	1112	0.64
		3680.0	0.76	3680.1	0.81	1112	0.67	1223	0.55
				3681.5	0.06	1110	0.68	1201	0.50
		3686.5	0.12	3685.1	0.11	1111	0.95	1222	0.62
				3691.2	0.16	2002	0.67	2113	0.48
		3698.5	1.34	3698.6	1.31	1001	0.80	1110	0.64
		3703.9	1.38	3704.0	1.70	1001	0.80	1111	0.94
3710.8	23.45	3710.9	8.14	3711.1	7.94	0000	0.95	0111	0.73
		3713.6	0.11	3713.7	0.19	1112	0.67	1222	0.62
		3716.9	0.46	3716.4	0.19	1110	0.68	1221	0.67
				3717.4	0.12	2002	0.67	2111	0.54
		3727.7	3.24	3727.4	2.27	0111	0.74	0222	0.48
		3737.0	0.56	3736.6	0.46	0111	0.74	0200	0.56
		3740.9	1.43	3740.4	1.97	1001	0.80	2002	0.66
		3743.8	0.20	3742.6	0.27	1111	0.95	2112	0.63
				3758.5	0.07	1111	0.95	2111	0.54
		3761.8	0.32	3760.9	0.21	1112	0.67	2113	0.48
				3913.8	0.02	0111	0.74	1310	0.42
3906.7	1.05	3906.8	0.45	3906.7	0.41	0000	0.95	1201	0.50
				3986.9	0.02	1001	0.80	1310	0.42
3988.9	1.600	3988.9	0.62	3989.6	0.53	0000	0.95	2111	0.54
				3992.8	0.03	1001	0.80	1311	0.51
				3997.7	0.007	1111	0.95	1422	0.38
				4144.4	0.008	0111	0.74	0400	0.36
		4149.9	0.40	4149.9	0.27	1001	0.8	3112	0.64

TABLE III. First 20 calculated energy levels of *para*-D_2@C_{60} for the ground ($v=0$) and excited ($v=1$) states. The excitation energies ΔE^0_{para} and ΔE^1_{para} (in cm^{-1}) are relative to the ground-state energy E^0_{1001} = 1696.21 cm^{-1} and E^1_{1001} = 4618.18 cm^{-1}. $|\xi^v|^2$ is the contribution of the dominant quantum basis $|JNL\Lambda\rangle$ to the particular eigenstate.

$v=0$			$v=1$		
$JNL\Lambda$	ΔE^0_{para}	$\lvert\xi^0\rvert^2$	$JNL\Lambda$	ΔE^1_{para}	$\lvert\xi^1\rvert^2$
1001	0.0	0.99	1001	0.0	0.99
1111	122.9	0.97	1111	123.1	0.97
1112	126.6	0.97	1112	127.5	0.96
1110	132.3	0.96	1110	134.7	0.96
1222	254.0	0.94	1222	255.2	0.93
1223	259.0	0.93	1223	261.1	0.90
1221	259.5	0.70	1221	261.6	0.65
1201	271.2	0.67	1201	275.4	0.61
3003	292.6	0.98	3003	282.1	0.96
1333	390.5	0.90	1333	393.0	0.87
1334	396.4	0.86	1334	398.6	0.70
1332	397.6	0.76	1332	401.6	0.71
1311	406.2	0.83	3113	404.8	0.94
1312	413.6	0.61	1311	410.2	0.80
3113	415.3	0.97	3112	410.8	0.86
3114	420.4	0.93	3114	412.7	0.75
1310	421.1	0.81	1312	421.9	0.59
3112	422.0	0.85	1310	428.6	0.78
1444	536.6	0.85	3224	536.9	0.78
1445	542.2	0.65	3223	537.5	0.83

levels of HD@C_{60} is very different from H_2@C_{60} and D_2@C_{60} due to strong mixing of states. However, for all three isotopomers only the states with the same Λ are mixed, if the potential is spherical.

Some of the lines in the 90 K spectrum or at lower T show small splittings: the 3056.8 cm^{-1} and 3224.4 cm^{-1} lines in D_2@C_{60} (Fig. 4(b)) and the 3698.5 cm^{-1}, 3710.8 cm^{-1}, 3906.7 cm^{-1}, and 3988.9 cm^{-1} lines in HD@C_{60} (Fig. 3). These splittings are not described by our model, which assumes local spherical symmetry, and the split lines are treated as single experimental lines in the fit. As discussed before[9] in the case of H_2@C_{60}, the local icosahedral symmetry of the C_{60} cage is too high to give rise to such splittings. The shape of spectral lines showing this type of splitting is very similar in H_2@C_{60}, D_2@C_{60}, and even in HD@C_{60}. This splitting is independent of the isotopomer and depends on the initial and/or on the final state defined by quantum numbers v, J, N, L, and Λ.

V. DISCUSSION

A. Hamiltonian parameters

The potential parameters ${}^vV^{ljn}_{00}$ and vibration-rotation Hamiltonian parameters, ω_0, B_e, α_e, and D_e, are listed in Table VI for all three isotopomers. The harmonic ${}^vV^{002}_{00}$ and anharmonic ${}^vV^{004}_{00}$ part of the isotropic potential are

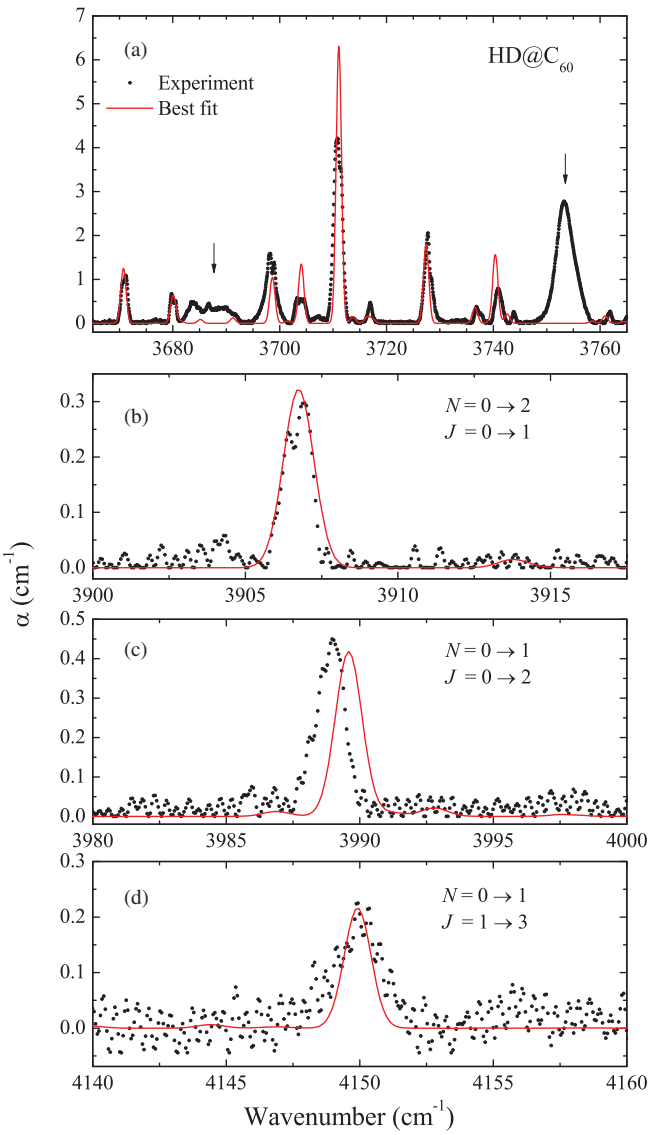

FIG. 7. Experimental absorption spectra of HD@C_{60} at 90 K (dots) together with the fit result with fixed line width, FWHM = 1 cm^{-1}. The changes of the quantum numbers J and N for the transitions in panel (a) vary from line to line and are $\Delta J = 0$, $\Delta N = 1$, or $\Delta J = 1$, $\Delta N = 0$. Some lines in the experimental spectrum do not belong to HD and are indicated by arrows.

TABLE IV. Calculated energy levels of *ortho*-D_2@C_{60} for the ground ($v = 0$) and excited ($v = 1$) states up to $JNL\Lambda = 4113$. The excitation energies ΔE^0_{ortho} and ΔE^1_{ortho} (in cm^{-1}) are relative to the ground-state energy $E^0_{0000} = 1637.56$ cm^{-1} and $E^1_{0000} = 4561.71$ cm^{-1}. $|\xi^v|^2$ is the contribution of the dominant quantum basis $|JNL\Lambda\rangle$ to the particular eigenstate.

$v = 0$			$v = 1$		
$JNL\Lambda$	ΔE^0_{ortho}	$\lvert\xi^0\rvert^2$	$JNL\Lambda$	ΔE^1_{ortho}	$\lvert\xi^1\rvert^2$
0000	0.0	0.99	0000	0.0	0.99
0111	125.9	0.97	0111	126.7	0.96
2002	175.7	0.99	2002	169.2	0.98
0222	258.1	0.94	0222	260.2	0.93
0200	268.0	0.90	0200	270.8	0.88
2112	298.7	0.97	2112	292.3	0.97
2113	302.5	0.97	2113	297.0	0.96
2111	305.0	0.96	2111	300.2	0.96
0333	395.7	0.90	0333	399.6	0.88
0311	410.8	0.82	0311	415.7	0.79
2223	430.5	0.94	2223	425.4	0.93
2222	431.3	0.84	2222	426.3	0.81
2224	435.3	0.93	2224	431.3	0.92
2221	437.1	0.94	2221	433.5	0.92
2220	440.4	0.93	2220	437.8	0.92
2202	445.6	0.80	2202	442.6	0.77
0444	543.8	0.89	0444	552.0	0.88
2334	567.8	0.90	4004	562.0	0.98
2333	568.0	0.86	2334	564.3	0.89
0422	568.2	0.78	2333	564.6	0.83
2332	572.0	0.80	2332	569.3	0.75
2335	573.5	0.89	2335	571.2	0.88
2331	577.8	0.88	2331	576.8	0.86
0400	579.1	0.74	0422	579.5	0.76
2312	583.2	0.74	2312	581.3	0.68
4004	583.6	0.99	2313	588.7	0.74
2313	589.3	0.78	0400	591.9	0.71
2311	592.4	0.80	2311	592.5	0.77
0555	696.7	0.86	4114	684.9	0.96
4114	706.5	0.97	4115	690.5	0.96
4115	710.9	0.97	4113	691.9	0.96
4113	712.0	0.97	0555	709.1	0.85

similar for three isotopomers. There is a slight trend that these two parameters are larger for the heavier isotopomers. If the separation of two energy levels, $E^1_{01111} - E^1_{0000}$ is accounted for in *ortho*-D_2@C_{60}, 126.7 cm^{-1} (Table IV), and in *para*-H_2@C_{60},184.4 cm^{-1} ,[9] we get the ratio 1.4566, which is larger than the mass scaling, $\sqrt{m_{D_2}/m_{H_2}} = \sqrt{2}$. This tells us that the splitting of energy levels is larger in H_2@C_{60} even though the potential parameters are smaller. The controversy is resolved if one takes into account the anharmonic energy correction to the difference $E^1_{01111} - E^1_{0000}$. Beside the dependence on ${}^vV^{002}_{00}$ and ${}^vV^{004}_{00}$, which are larger for D_2, the linear energy correction in the perturbation theory to this difference decreases with the increase of the molecular mass as $m^{-0.5}$.

The displacement of the center of mass from the bond center changes the dynamics of HD in the C_{60} cage drastically. In our model, this change is represented by the ${}^vV^{111}_{00}$ and ${}^vV^{113}_{00}$ potential parameters. These potential terms shift the HD center of mass away from the cage center. HD cannot rotate in the cage unless the center of mass is moving along the circular trajectory, in a classical view. The rotational quantum number J is not a good quantum number any more.[8] The spherical symmetry is preserved and Λ ($\mathbf{\Lambda} = \mathbf{L} + \mathbf{J}$) is still a good quantum number.

The rotational and translational states are mixed in quantum mechanical terms. As an example, we analyze three states where the main component is $N = 0$ and $J = 0, 1$, or 2. It was pointed out in the INS study that the energies of these levels do not scale as is expected for the rotational states of a diatomic rotor.[10] Our fit shows that the $J = 1$ state of HD has 80% $J = 1$, $N = 0$, $L = 0$ component, Table V, and the next main component with 18% weight has quantum numbers $J = 0$, $N = 1$, $L = 1$. The linear potential ${}^vV^{111}_{00}$ couples the two components and they both have $\Lambda = 1$. The next rotational level is 67% of $J = 2$, $N = 0$, $L = 0$, and 28% of $J = 0$, $N = 2$, $L = 2$. Here, the ${}^vV^{111}_{00}$ has zero matrix element between the two components. However, the coupling goes

TABLE V. Calculated energy levels of HD@C_{60} for the ground ($v = 0$) and excited ($v = 1$) states up to $JNL\Lambda = 3112$. The excitation energies ΔE^0_{HD} and ΔE^1_{HD} (in cm^{-1}) are relative to the ground-state energy $E^0_{0000} = 1964.05$ cm^{-1} and $E^1_{0000} = 5517.66$ cm^{-1}. $|\xi^v|^2$ is the contribution of the dominant quantum basis $|JNL\Lambda\rangle$ to the particular eigenstate.

$v = 0$			$v = 1$		
$JNL\Lambda$	ΔE^0_{HD}	$\lvert\xi^0\rvert^2$	$JNL\Lambda$	ΔE^1_{HD}	$\lvert\xi^1\rvert^2$
0000	0.0	0.95	0000	0.0	0.94
1001	80.3	0.80	1001	76.6	0.80
0111	153.3	0.74	0111	157.5	0.73
1112	202.4	0.67	1112	197.4	0.64
1110	225.2	0.68	1110	225.3	0.64
1111	231.0	0.95	1111	230.6	0.94
2002	272.1	0.67	2002	267.0	0.66
0222	318.1	0.47	0222	327.2	0.48
0200	324.0	0.61	1223	328.9	0.55
1223	334.5	0.59	0200	336.3	0.56
1201	357.5	0.51	1201	353.1	0.50
1222	365.4	0.70	1222	362.6	0.62
1221	384.0	0.70	1221	388.0	0.67
2113	413.3	0.54	2113	409.8	0.48
2112	420.6	0.72	2112	420.0	0.63
2111	432.6	0.60	2111	436.0	0.54
1334	474.7	0.53	1334	468.5	0.49
0333	481.0	0.44	0333	489.8	0.37
0311	500.1	0.44	1312	495.6	0.44
1312	501.2	0.46	1333	503.8	0.48
1333	507.5	0.56	1310	513.5	0.42
1310	515.7	0.46	1311	519.4	0.51
1311	522.6	0.54	0311	519.7	0.39
3003	533.3	0.83	3003	525.6	0.58
1332	535.6	0.54	1332	537.9	0.38
2224	562.8	0.43	2224	560.0	0.35
2222	565.5	0.57	2222	569.2	0.42
2223	575.3	0.50	1333	578.1	0.38
2202	588.8	0.33	2202	590.9	0.22
2220	594.6	0.52	2220	605.2	0.46
2221	600.3	0.49	2221	613.0	0.44
1445	628.1	0.45	2335	620.6	0.44
0444	652.0	0.42	2334	653.7	0.50
2334	658.0	0.45	2313	653.8	0.4 0
1423	661.1	0.38	3114	655.0	0.49
3113	667.8	0.88	3113	656.7	0.81
3112	677.3	0.62	2311	675.1	0.49
1422	678.6	0.41	1422	675.1	0.38
2311	680.8	0.48	3112	676.6	0.64

over an intermediate state what is 67% $J = 1, N = 1, L = 1$, 15% $J = 0, N = 2, L = 2$, and 15% $J = 2, N = 0, L = 0$. These states are $\Lambda = 2$ states.

The potential terms ${}^vV^{111}_{00}$ and ${}^vV^{113}_{00}$ shift the HD center of mass from the C_{60} cage center. Using the potential values from Table VI we find that the minimum of the HD potential in the $v = 0$ state is shifted 0.1383 Å along the bond and in the $v = 1$ state by 0.1387 Å. Using the free HD bond length $s_0 = 0.74142$ Å (Ref. 18) we get for the deuteron distance from the cage center 0.3560 Å and for the proton distance 0.3854 Å in the ground vibrational state. The corresponding distances from the center of mass of free HD molecule are 0.24714 Å and 0.49428 Å. As one can see, inside C_{60} the two nuclei are placed fairly symmetrically relative to the cage center.

Another feature of HD is an enlarged anisotropic potential ${}^vV^{222}_{00}$, Table VI. ${}^vV^{222}_{00}$ is defined in the coordinate system where the rotation of the HD molecule is about its center of mass.

The relative change of the rotational constant is similar in H_2 and D_2 with respect to free molecule value. B_e depends on the nucleus-nucleus distance what is determined by electron-electron interactions. Since the electron-electron interactions, in the first approximation, are same for the two isotopomers, the relative change of B_e is independent of mass.

Among the rotation and vibration constants of HD@C_{60}, the centrifugal correction D_e to the rotational constant B_r, $B_r = B_e - \alpha_e(v + 1/2) - D_e J(J + 1)$,[9,18] is anomalously different from its gas phase value compared to other two isotopomers, Table VI. Positive D_e means that the faster the molecule rotates, the longer is the bond. We speculate that since the rotation center of HD inside the cage is further away from the deuteron, the centrifugal force on the deuteron increases and the bond is stretched more than in the free HD molecule.

B. Dipole moment

The dipole moment parameters A^{ljn} are listed in Table VI. A^{101} and A^{121} coefficients are the largest for the lightest isotopomer. These coefficients do not have explicit dependence on the vibrational coordinate and were defined in Eq. (2) as ${}^{v'v}A^{ljn} = \langle\psi^{vib}_{v'}(s)|A^{ljn}(s)|\psi^{vib}_{v}(s)\rangle$. We expand the coefficients in powers of $\delta s = s - s_0$ at the bond length s_0, $A^{ljn}(s) = A^{ljn}(s_0) + \frac{d}{ds}A^{ljn}|_{s_0}\delta s + \ldots$. The second term of this expansion gives the $v = 0 \to 1$ transition, $\langle\psi^{vib}_1(s)|s|\psi^{vib}_0(s)\rangle \sim \mu^{-0.25}$ where μ is the reduced mass of the hydrogen molecule.[3] The ratio of the A^{101} coefficients of H_2 and D_2 is ~1.3, Table VI. This is not very different from the estimate using the reduced masses, $2^{0.25} \approx 1.19$. The ratio of the anisotropic coefficients, A^{121}, is almost 1.5, however with the large error bar dominated by the error of the D_2 coefficient.

We found that in the D_2 sample several absorption lines were rendered invisible. There are other factors, beside the A coefficients dependence on the vibrational coordinate, that reduce the D_2@C_{60} IR line intensities compared to H_2@C_{60}. From Eq. (17) of Ref. 9, we get that the line area is $S(\omega) \sim \omega(A^{lj1})^2|\langle\psi^1_{N=1}|R|\psi^0_{N=0}\rangle|^2$. The matrix element of the radial part depends on the molecule mass as $|\langle\psi^1_{N=1}|R|\psi^0_{N=0}\rangle|^2 \sim m^{-0.5}$, Ref. 3. The transition frequency ω is approximately equal to the vibrational frequency $\omega_0 \sim \mu^{-0.5}$. If one uses 1.3 as the experimental ratio of the A^{101} coefficients of H_2 and D_2, the estimate of the relative line intensities of the two isotopomers is $S_{H_2}/S_{D_2} = 3.3$.

While the coefficients A^{101} and A^{121} are zero for the free hydrogen molecule, the third coefficient A^{010}, allowed by symmetry in a heteronuclear diatomic, describes the dipole moment of a rotating molecule. However, inside C_{60} it could be different from the free HD value. The permanent dipole

TABLE VI. Values of the fitted parameters κ_i for HD and D_2@C_{60} compared to the results for H_2@C_{60} (Ref. 9). The vibrational and rotational constants of a free molecule of the three hydrogen isotopomers are shown for comparison; gas phase ω_0 is calculated including all terms $(v+1/2)^k$ up to $k=3$ (Ref. 18). In HD@C_{60} and D_2@C_{60} the parameter ${}^{v}V_{00}^{224}$ is set to zero. Currently and previously used dipole moment expansion parameters are related as ${}^{v'v}A^{lj1} = 20B_{v'v}[lj]$, where $B_{v'v}[lj]$ is the pairwise H_2-carbon induced dipole moment expansion parameter given by Eqs. (13) and (14) in Ref. 9.

	H_2@C_{60}		HD@C_{60}		D_2@C_{60}		
κ_i	$v=0$	$v=1$	$v=0$	$v=1$	$v=0$	$v=1$	Unit
${}^{v}V_{00}^{002}$	14.277 ± 0.034	15.952 ± 0.032	16.355 ± 0.065	17.483 ± 0.048	16.781 ± 0.080	16.456 ± 0.056	Jm^{-2}
${}^{v}V_{00}^{004}$	$(2.2105 \pm 0.0099)10^{21}$	$(2.1920 \pm 0.0085)10^{21}$	$(1.884 \pm 0.024)10^{21}$	$(2.133 \pm 0.015)10^{21}$	$(2.159 \pm 0.041)10^{21}$	$(2.390 \pm 0.022)10^{21}$	Jm^{-4}
${}^{v}V_{00}^{222}$	0.5629 ± 0.0059	1.199 ± 0.012	1.313 ± 0.040	2.037 ± 0.058	1.11 ± 0.22	1.40 ± 0.14	Jm^{-2}
${}^{v}V_{00}^{224}$	$(2.211 \pm 0.023)10^{20}$	$(1.030 \pm 0.011)10^{20}$	0	0	0	0	Jm^{-4}
${}^{v}V_{00}^{111}$	...	...	$(3.1102 \pm 0.0095)10^{-10}$	$(3.251 \pm 0.010)10^{-10}$	...	...	Jm^{-1}
${}^{v}V_{00}^{113}$	...	...	$(4.25 \pm 0.18)10^{10}$	$(7.12 \pm 0.11)10^{10}$	...	...	Jm^{-3}
n_o/n_p	2.890 ± 0.045		—		2		
A^{010}	—		$(-1.54 \pm 0.15)10^{-32}$		...		Cm
A^{101}	$(9.06 \pm 0.26)10^{-22}$		$(7.01 \pm 0.69)10^{-22}$		$(6.85 \pm 0.73)10^{-22}$		C
A^{121}	$(-4.26 \pm 0.42)10^{-22}$		$(-2.67 \pm 0.27)10^{-22}$		$(-2.9 \pm 1.5)10^{-22}$		C
	H_2@C_{60}	H_2	HD@C_{60}	HD	D_2@C_{60}	D_2	
ω_0	4062.37 ± 0.28	4161.18	3549.66 ± 0.39	3632.20	2924	2993.69	cm^{-1}
B_e	59.865 ± 0.074	60.853	45.38 ± 0.14	45.655	29.888 ± 0.089	30.444	cm^{-1}
α_e	2.974 ± 0.025	3.062	1.695 ± 0.044	1.986	1.086 ± 0.045	1.079	cm^{-1}
D_e	$(4.832 \pm 0.051)10^{-2}$	4.71×10^{-2}	$(1.535 \pm 0.097)10^{-1}$	2.605×10^{-2}	$(8.45 \pm 3.71)10^{-3}$	1.141×10^{-2}	cm^{-1}

moment of the free HD molecule corresponding to the $v=0 \rightarrow 1$, $J=0 \rightarrow 1$ transition is 5.0×10^{-5} D,[20] while the endohedral HD dipole moment is $|A^{010}| = 1.54 \times 10^{-32}$ Cm $= 4.77 \times 10^{-3}$ D, Table VI. The dipole moment A^{010} of HD inside C_{60} is enhanced by two orders of magnitude because of the mutual induced polarization of HD and C_{60}.

Despite the enhancement of the rotational dipole moment A^{010} we did not detect the rotational transition $J=0 \rightarrow 1$, $\Delta N = 0$ in the IR spectra of HD@C_{60}. Indeed, our model fit gives a rather small area $S = 0.07$ cm^{-2} for this line at 3630.2 cm^{-1} and at temperature 5 K. The $\Delta J = 1$ transition in HD@C_{60} is suppressed because there is an interference of two dipole terms, A^{010} and A^{101} which have opposite signs. The final state consists of 80% of pure rotational state $J=1$, $N=0$ and 18% of the pure translational state $N=1$, $J=0$, Table V. This mixed final state has matrix elements from the ground state for both A coefficients, A^{010} and A^{101}, which nearly cancel each other.

Olthof *et al.* did not consider induced dipole moments in CO@C_{60}.[16] Their approach is probably justified as free CO has large rotational and vibrational dipole moments and the induced moments are relatively small. Our study shows that in HD@C_{60} the induced rotational and translational dipole moments are both equally important in rotational transitions and two orders of magnitude larger than the permanent rotational dipole moment of HD.

VI. SUMMARY

We measured and analyzed the infrared absorption spectra of D_2@C_{60} and HD@C_{60} and compared the results to H_2@C_{60}. The rotation and translation transitions appear in combination with the fundamental vibrational transition, $v=0 \rightarrow 1$. Experimentally, the two heavier hydrogen isotopomers are more challenging than H_2. Several IR absorption lines were missing in D_2@C_{60} and HD@C_{60} spectra, including the fundamental vibrational transition. Heavier mass reduces the IR line intensity through several parameters and in addition, shifts spectra to lower frequency where the background absorption of the C_{60} powder is stronger and, as a consequence, the signal-to-noise ratio is reduced.

The potential parameters of H_2 and D_2 show little mass dependence. This is true for the isotropic part of the HD potential ${}^{v}V_{00}^{002}$ as well. Absence of the inversion symmetry in HD allows additional potential parameters, ${}^{v}V_{00}^{111}$ and ${}^{v}V_{00}^{113}$, which mix the rotational levels and J is not a good quantum number any more. This is the effect of the confining potential what prohibits the rotation of the HD molecule about its center of mass, as predicted for HD@C_{60} (Ref. 8) and for another endohedral complex without the center of inversion, CO@C_{60}.[16]

In HD@C_{60} the dipole moment A^{010} for rotational transition $v=0 \rightarrow 1$, $J=0 \rightarrow 1$ with $\Delta N = 0$ is enhanced by two orders of magnitude compared to the free HD molecule value. However, because the final state is not a pure $J=1$ state, the interference with the induced dipole moment term A^{101} renders this IR transition invisible in our measurement.

The accuracy of the potential could be improved further by measuring the IR fundamental vibrational and the $\Delta N = -1$ transitions, and transitions to higher N levels in HD@C_{60} and D_2@C_{60} with better signal-to-noise ratio. This could be achieved by using samples in the shape of a single crystal, few mm in size. In addition, a single crystal study would shed some light on the splitting of some $\Lambda < 3$ levels and increase the accuracy of the dipole moment parameters as there would be no light scattering such as in the powder sample. However, this would increase the predictive power of our model for higher N values only. The separation and

translation-rotation splitting of the lowest N levels already detected in the experiment would not change, especially in the HD sample where additional information from the INS experiment[10] was used to compensate for the missing fundamental transition.

ACKNOWLEDGMENTS

We thank Professor Pekka Pyykko for helpful discussions. This research was supported by the Estonian Ministry of Education and Research Grant No. SF0690029s09, Estonian Science Foundation Grant Nos. ETF7011, ETF8170, JD187. We thank Engineering and Physical Sciences Research Consul (U.K.) (EPSRC(GB)) and the Royal Society (UK) for support.

[1]K. Komatsu, M. Murata, and Y. Murata, Science **307**, 238 (2005).
[2]M. Murata, Y. Murata, and K. Komatsu, J. Am. Chem. Soc. **128**, 8024 (2006).
[3]S. Flügge, *Practical Quantum Mechanics* (Springer-Verlag, Berlin, 1971), Vol. 1.
[4]S. Mamone, M. Ge, D. Hüvonen, U. Nagel, A. Danquigny, F. Cuda, M. C. Grossel, Y. Murata, K. Komatsu, M. H. Levitt, T. Rõõm, and M. Carravetta, J. Chem. Phys. **130**, 081103 (2009).
[5]R. J. Cross, J. Phys. Chem. A **105**, 6943 (2001).
[6]T. Yildirim and A. B. Harris, Phys. Rev. B **66**, 214301 (2002).
[7]M. Xu, F. Sebastianelli, Z. Bačić, R. Lawler, and N. J. Turro, J. Chem. Phys. **128**, 011101 (2008).
[8]M. Xu, F. Sebastianelli, Z. Bačić, R. Lawler, and N. J. Turro, J. Chem. Phys. **129**, 064313 (2008).
[9]M. Ge, U. Nagel, D. Hüvonen, T. Rõõm, S. Mamone, M. H. Levitt, M. Carravetta, Y. Murata, K. Komatsu, J. Y.-C. Chen, and N. J. Turro, J. Chem. Phys. **134**, 054507 (2011).
[10]A. J. Horsewill, S. Rols, M. R. Johnson, Y. Murata, M. Murata, K. Komatsu, M. Carravetta, S. Mamone, M. H. Levitt, J. Y.-C. Chen, J. A. Johnson, X. Lei, and N. J. Turro, Phys. Rev. B **82**, 081410 (2010).
[11]M. Xu, F. Sebastianelli, B. R. Gibbons, Z. Bačić, R. Lawler, and N. J. Turro, J. Chem. Phys. **130**, 224306 (2009).
[12]S. Mamone, J. Y.-C. Chen, R. Bhattacharyya, M. H. Levitt, R. G. Lawler, A. J. Horsewill, T. Rõõm, Z. Bačić, and N. J. Turro, Coord. Chem. Rev. **255**, 938 (2011).
[13]J. M. Brown and A. Carrington, *Rotational Spectroscopy of Diatomic Molecules* (Cambridge University Press, Cambridge, England, 2003).
[14]N. J. Turro, J. Y. C. Chen, M. Sartori, E.; Ruzzi, A. A. Marti, R. G. Lawler, S. Jockusch, J. López-Gejo, K. Komatsu, and Y. Murata, Acc. Chem. Res. **43**, 335 (2010).
[15]N. J. Turro, A. A. Marti, J. Y.-C. Chen, S. Jockusch, R. G. Lawler, M. Ruzzi, E. Sartori, S.-C. Chuang, K. Komatsu, and Y. Murata, J. Am. Chem. Soc. **130**, 10506 (2008).
[16]E. H.T. Olthof, A. van der Avoird, and P. E. S. Wormer, J. Chem. Phys. **104**, 832 (1996).
[17]S. L. Altmann and P. Herzig, *Point-Group Theory Tables* (Oxford University Press, Oxford, 1994).
[18]K. P. Huber and G. Herzberg, *Constants of Diatomic Molecules. IV. Molecular Spectra and Molecular Structure* (Reinhold, New York, 1979).
[19]A. D. Buckingham, Trans. Faraday Soc. **56**, 753 (1960).
[20]N. H. Rich, J. W. C. Johns, and A. R. W. McKellar, J Mol. Spectrosc. **95**, 432 (1982).